Geometric Improvement of a Perimetric Exhaust

Miguel Alexandre Fechado
miguel.fechado@tecnico.ulisboa.pt

Instituto Superior Técnico, Universidade de Lisboa, Portugal

November 2019

Abstract

The following work focuses on the improvement of the channel geometry inside a perimetric exhaust, with the goal of improving the energetic and grease filtering performance. This is done via numerical simulations, with an experimental part to assess the results obtained computationally. The initial geometry was studied to act as an initial point of comparison to the first geometry variation, as well as to determine how different characteristics of the flow (recirculation zones) vary with different inlet velocities and working temperatures. Then, two first variations were tested, both improving on the initial basis. The best one from those two went through another three iterations to maximize the improvement by reducing local losses and grease depositing in the walls. All of the three new versions improved on the already upgraded geometry, with the reduction and eventual elimination of the bottom recirculation zone having a great effect both in terms of energetic efficiency and also on the capacity to direct the grease particles to the filter, as desired. In addition, a new real geometry implemented in the same exhaust was studied and compared to the initial, in order to assess the behaviour of this new version. An experimental test was also made, where a new method to collect pressure loss data was proved fruitful and a correlation was obtained between the experimental and numerical results, with the values being close enough to verify the quality of the numerical part.
Keywords: Perimetric exhaust, Right-angled channel, Turbulent flow, Grease deposition

1. Introduction

1.1. Motivation

The importance of environmental measures has been increasing in the past few years. With climate change becoming more real each year that goes by, energetic improvements are discussed and made in every single possible way. Household appliances are no exception to it, including kitchen exhausts. These machines perform a very important task as they clean up the air during cooking tasks. Energetic consumption and grease filter efficiency are between the 4 classes evaluated and classified by a set of rules created by the European Commission. They also oblige the exhaust to go through several standard tests with a final overall grade. With more demanding standards to be released soon, a decrease in classification comes for companies that do not upgrade the performance of their kitchen exhausts. It represents an opportunity for companies to be up to the state of art and a chance for house-owners to purchase a more environmental friendly device.

For this reason, the optimization of perimetric exhausts is of great interest for both industry and its costumers. Hence, this work has the objective of improving the energetic performance of the perimetric exhaust being studied, while controlling and trying to direct the grease particles contained in the flow to the desired location: the filters, avoiding its deposition in the exhaust's walls.

1.2. Theoretical Overview

This thesis focuses on the specific behaviour of perimetric exhausts, both in terms of the flow dynamics and the particles it contains. This type of exhausts are characterized by not having the filters right next to the air intake, in direct contact with the kitchen environment. Instead, the air is directed through a small gap that goes all around the extremity of the exhaust, being diverted inside to its centre, where the filter is, as it is show in Figure 1.

Figure 1: Cross-section representation of a perimetric exhaust (adapted from [1]).

While this has the advantage of improving the Indoor Air Quality (IAQ) of the room, it comes with disadvantages. The deflection imposed to the

flow in the channels by the 90 degree angle after the entrance implies a loss of energy before reaching the fan that other exhausts do not have, turning it into a less efficient exhaust. In addition, the tightness of the channel and its corner may imply that not all of the particles contained in the flow pulled by the fan reach the filter. In a worst case scenario, this might result in some grease slipping to the entry gap and even dripping to the exterior.

This work simplifies the geometry of a perimetric exhaust to a bi-dimensional channel representing one of the sides of the exhaust, in order to obtain results in a less computationally expensive. The inlet channels are the cause for the complexity of this problem. The sharp angles present in the geometries of this work create large pressure gradients after the corner, which results in flow separation and therefore a loss of energy from the flow. A narrow entrance allows for considerable inlet velocities, with Reynolds number values in (or near) the turbulent region. The sharp edges presented to the flow would always result in its transition to turbulent, even if the entry values are lower [2]. Therefore, the flow throughout this work was considered to be fully turbulent. Without being able to change the entrance area or shape, in order to keep the same flow rate and suction capacity from the exhaust and avoiding any new molds for its manufacturing, this work will apply simple geometric changes to the sharp-edged zone in order to mitigate this effect. Due its shape, the exhaust channels can be related to a piping system. According to [3], the losses in a pipe flow can be divided into two types: friction losses and local losses. In this work, local losses are the main topic since that is how most of the energy is removed from the flow. They refer to, as the name says, local effects created due to disturbances to the natural track of the flow. To evaluate local losses in duct flows and compare similar cases, it is used a dimensionless value: the local pressure loss coefficient, K. The value of the coefficient for a certain case reflects how big the pressure loss is in the corresponding zone of analysis: higher K corresponds to a bigger energy loss. A theoretical definition is shown in Equation 1 [3].

$$K = \frac{h_m}{\frac{{V_m}^2}{2g}} = \frac{\Delta p}{\frac{1}{2}\rho {V_m}^2} \tag{1}$$

Although the heat from the stove is supposed to be transferred to the food being cooked, some losses end up occurring in the system during the activity. For this reason, studying how the temperature affects the flow parameters and characteristics inside the channel is also important to the present work.

The flow inside an exhaust has a distinguished complexity not only because of the channel geometries perimetric exhausts have, but also because the non-isothermal flow inside is not just purely air but a mix from the cooking activities performed underneath the exhaust, mainly composed by water vapour and grease particles [4]. The mass changes from particle to particle, enough to affect their movement and can be characterized by the dimensionless Stokes number, St (Equation 2), with smaller Stokes number representing a small particle, and a bigger particle have a bigger Stokes number. Particles with a lower St tend to follow the streamlines from the flow they are in while a bigger Stokes number means they can leave recirculation zones and vortexes due to their inertia [5].

$$St = \frac{\rho_p {D_p}^2/18\mu_f}{D_0/U_0} = \frac{\tau_\mathrm{p}}{\tau_\mathrm{L}} \tag{2}$$

2. Methodology and Experimental Setup

The thesis focuses on studying the two-phase flow inside the channels of an exhaust and how to improve its performance by optimizing their geometry. For that, numerical simulations following up to the work of Monteiro [2], were carried out changing several parameters in order to analyse how it affects the pressure losses and particle deposition. An experimental setup was adapted from the work of Ferro [6] to assess the results obtained numerically.

The exhaust analysed in this study is a perimetric exhaust. This type of exhausts are characterized by an entry slot that goes all around the near-edge of its inferior surface, as it was previously shown in Figure 1, giving access to the channels being studied. The exhaust has 3 different working powers corresponding to three different air mass flows, that is, three inlet velocities.

2.1. Software and Numerical Simulation Overview

The exhaust was studied numerically in a multiphysics commercial software: *COMSOL MULTIPHYSICS®*. The use of this software allows to simulate several physics in different studies, some at the same time. Since this case covers several types of studies (heat transfer, fluid dynamics and particle tracing), this makes it the ideal program to run the studies related to this work. The numerical simulations focus mainly on the corner of the exhaust's channel. The geometries studied have their inlet at the entry of the channel, and their outlet far enough so that the measurements are not influenced by the pressure disturbances coming from the corner where the flow returns to a fully developed state. Several different geometries were put into test to verify how they were impacted by different velocities and by changes in the flow temperature. Ergo, code names were created in order to easily identify each of the different geometries. The study begins with geometry A (Figure 2), equivalent to the real initial geometry of the exhaust, analysed in

the studies that preceded this work [6, 2].

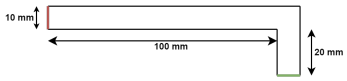

Figure 2: Representation of geometry A.

Two new geometries followed as a starting point for the geometry improvement of the channel: geometries B and C (Figure 3). Both geometries represent a small change to the initial, allowing them to be produced without big changes to the manufacturing process, as desired by the company that produces these perimetric exhausts.

Figure 3: Representation of geometries B and C.

In the following step of the process, three variations from geometry B were studied: geometries B15, B20 and B30. The codes names reflect their characteristics: B tells that the geometry is a version based on geometry B, and the number represents the distance in which the inside corner point was moved to the left, from its original spot.

Recently, some adjustments in the exhaust's manufacturing led to a considerable change in the channel geometry. Hence, it was decided to run new studies with the most recent geometry, named geometry D (Figure 4), to see how it affects the particle deposition and the pressure losses in the exhaust system. For reasons later clarified, it was also created a second geometry, geometry E, equal to geometry D but with the outlet further 150 mm away from the outlet of geometry D. The last geometries studied were an improvement of geometry E equivalent to geometry B and its improvement.

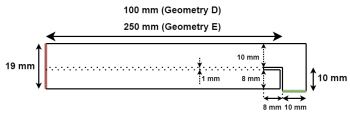

Figure 4: Representation of geometries D and E.

For all geometries referred to before, numerical studies were conducted to determine the local pressure losses and study the particle movement and deposition and also how the different inlet velocities and temperatures would change the characteristics and results. The two points to be studied, flow and particle analysis, were performed separately. Due to the nature of the flow simulation, which includes a heat transfer module to reproduce the effects of the heated air inside the channels, the simulations were made with compressible flow.

As seen in the previous work from Monteiro [2], the flow inside the channel was proven to be in turbulent conditions for ambient conditions, contrary to what was originally thought. After acknowledging that the flow to be studied was turbulent, a mathematical model was chosen in order to solve the problem. Making the study steady-state and averaging the properties of the flow saves a lot of calculations, reducing the computational time. This was done by the Reynolds-Averaged Navier-Stokes (RANS) model, which makes a statistical time average to the dependent variables of the Navier-Stokes equations: the Reynolds decomposition method. Since the compressibility element is present in the cases under analysis, the Navier-Stokes equations are composed of two balance equations (plus the energy equation) to be calculated by the solver: mass and momentum balance. To solve all of the unknowns in the equations above, a turbulence model is required. This will solve the Eddy viscosity, which acts as the responsible for momentum transfer. There exists several types of Eddy-viscosity models as well, with the 2-equation model k-ω being the chosen to this study. This model provides information about the turbulent kinetic energy, k, and the specific dissipation, ω.

At the walls, two conditions were set for the fluid flow module: an impermeability condition and a no-slip condition, since the study includes viscous flow. The walls were also considered to be hydraulically smooth. At the inlet, four different inlet velocities were studied, with a normal inflow profile. For the outlet, an uniform pressure condition was set at 0, with the reference level pressure being the atmospheric pressure. The solver was used a segregated one, with a termination criteria where the simulation ended by reaching an iteration error below 10^{-8}.

Being over a cooking stove means that the flow entering the exhaust may not be at ambient temperature, changing the air temperature moving into the channels and, with that, its properties. The numerical simulation of the exhaust takes this consideration into account by running the fluid flow simulations in a non-isothermal option. Similarly to the fluid flow part of the problem, the heat transfer part undergoes some simplifications: the flow is seen as a simple heat flow in a pipe. The wall boundaries have no thickness and are in contact with both the flow inside of the channel and with the ambient air outside the exhaust, at 20°C. Radiation is ignored and since the walls with no thickness in the simulation, there's also no conduction. This means that the only type of heat transfer considered in this numerical study is convection, more specifically, internal forced convection in the walls (Equation 3).

$$q_{wall} = h(T_{ext} - T) \quad (3)$$

In geometries D and E there is an extra condition being imposed, with the reversed L shaped empty zone, representing a tiny L, having no heat flux since the conduction there is negligible. For the Heat Transport turbulence model, the Kays-Crawford model was used.

Due to the cooking activities performed underneath the exhaust, this intakes a two-phase flow, composed by grease particles that can end up depositing inside the channels of the exhaust. Therefore, the particle movement had to be studied with the *Particle Tracing* module. This module can be used in this case, since the volume fraction of the solid phase (particles) is inferior to 1%. In the case of this work, due to the very small diameters of the particles, it is considered to be a sparse flow, where a one-way coupling is applied. This means that the particle phase movement is influenced by the continuous fluid flow phase, but the particles do not affect the fluid flow phase or each other due to their small volume.

For the case of this study, drag is the main force acting in the particles and influencing its movement, calculated by the Schiller-Naumann law. However, drag is not the only required force in the case of this work. Being a flow with considerate mass, the gravity force (F_g) must be also taken into account. With the study including near-walls to the flow, some studies were run to test the effect of shear induced lift forces on the particle movement and deposition. Despite that, it was seen that turbulent eddies excluded the effect, not being considered for the final calculations. Since the flow was turbulent, the effects it might provoke on the particles were also analysed via a turbophoretic force but the studies showed its application did not change the final result, being discarded. The heat flux coming from the stove and cooking tasks can also affect the particle motion via the thermophoretic force. However, it shouldn't affect the range of particles in this study. This range, influenced by the studies of [4] and [2], is between 10 and 100 μm, while the particle density (ρ_p) was kept equal to the one used by Monteiro[2], 980 kg/m^3. For the inlet it was established an uniform distribution for the particles along the 10 mm wide entry, with a batch of 100 particles being released each 0,04 seconds during a 1 second time span. To see the progress of the continuous depositing of the particles, the study was made time dependent, with a time step of 0,005 seconds and a total duration of 1,5 seconds. Each geometry was analysed for a set of 10, 15, 20, 25, 50 and 100 μm, with each diameter being studied separately for each different inlet velocity (V_{max} and V_{min}) and temperature(T = 20, 40 and 60°C).

2.2. Experimental Setup Overview

To evaluate some of the values obtained in the numerical part, this work adds an experimental part as a complement. The objective is to analyse the results and compare with the numerical part. This is done via an acrylic prototype, initially used by Ferro [6], which was slightly improved for this work. To the acrylic part, a convergent metal duct was bolted and connected to an electric fan (controlled by a VARIAC) by a hose. The electric fan, which had a nominal voltage of 230 V, was responsible for the air suction, simulating the same effect made by a similar fan in the real perimetric exhaust. Just like in the numerical study, the only losses assessed in this part of the work are the local pressure losses, evaluated by the same dimensionless parameter K, the local pressure loss coefficient. For that, pressure had to be monitored by a set of pitot tubes that were connected to a *Sensirion SDP1000-L* pressure sensor, which in its turn was connected to an *Arduino* microcontroller. When ready to be tested, the whole setup was put in a supportive structure (Figure 5) with extra supports in a table to make sure the hose is kept straight and the fan at the same level compared to the remaining setup. It was made sure that the flow near the entry zone would not be disturbed by the structure and that the channel was at the correct angle so it would not influence the results.

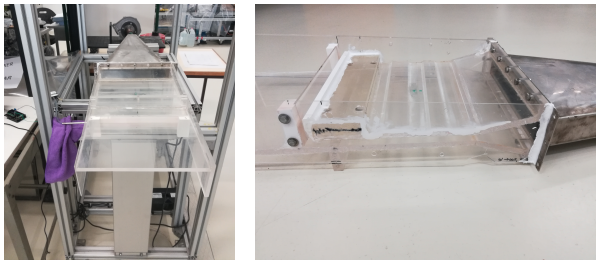

Figure 5: Experimental setup mounted in the structure (left) and in detail (right).

The static pressure data was retrieved in two different ways: by a single pitot tube further ahead in the channel comparing with the atmospheric pressure (*Single tube method*) and by two pitot tubes, one at the entry and the other in the channel (*Double tube method*). The ambient temperature of the room of did not affect the accuracy of the sensor and was controlled by a thermocouple. The experiment was made 10 times for each method, 5 for the maximum inlet velocity and 5 for the minimum inlet velocity, with data collected during a time interval of 15 seconds and processed in an Excel file.

3. Results

In this chapter, the results from both numerical and experimental parts of this work are presented.

Firstly, the numerical results are analysed, starting with the initial geometry, followed by all the alternatives. In each of them, the fluid flow is analysed first, followed by the particle studies, showing the results across the different temperatures and velocities. The numerical studies were all performed for the finer mesh, with an element side size of 0,1875 mm. The experimental part is then presented, with the analysis focused on pressure losses and comparing to the numerical case.

3.1. Initial Geometry

To begin this study, geometry A was analysed. This allows to see how the flow and its parameters change with the inlet velocity and temperature. This will also serve as a base result to compare with the following geometry improvements. One of the ways to reach the objective of this work is by analysing the pressures losses and flow parameters inside the geometry being studied. This can be done, as it was explained before, by checking the local pressure loss coefficient K for each case, inspecting as well what happens to the main causes for that pressure loss: the recirculation zones. This kind of geometries, with sharp corner angles, end up causing flow separation in two different recirculation zones: the *bottom recirculation zone*, in orange, and the *top corner recirculation zone*, in blue (Figure 6).

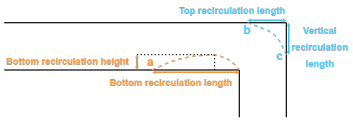

Figure 6: Basic layout for recirculation zones in geometry A (adapted from [6]).

In the top corner recirculation zone (TCR), the results show a clear tendency. Points b and c get closer to the corner when the inlet temperature increases and the velocity decreases. That was expected, since a higher temperature corresponds to a lower air density and with a lower velocity allow the flow adapts better to the geometry, reducing the size of the recirculation bubble. The results translate to a slightly bigger area for this recirculation zone with higher velocities, which is an equal outcome as it was obtained by Ferro [6]. For the bottom recirculation zone, the results make the analysis more complex since it shows that the bottom recirculation length has a peak value for a certain inlet temperature, depending on the velocity. Peak values for this length still increase with velocity but also increase with temperature, happening around the same interval in terms of Reynolds number (2350 to 2550). The existence of a recirculation zone after the corner induces a choking effect to the channel, reducing the useful height for the air flow and creating a bottleneck. The *bottom recirculation height* of the bubble was, then, also analysed. It was opted to check the results just for the some temperatures and for the minimum and maximum velocities, with peak values of around 4,5 mm occurring 12 mm to the left of the 90 degree corner and the results barely change with both velocity and temperature changes, following trends similar to Ferro [6].

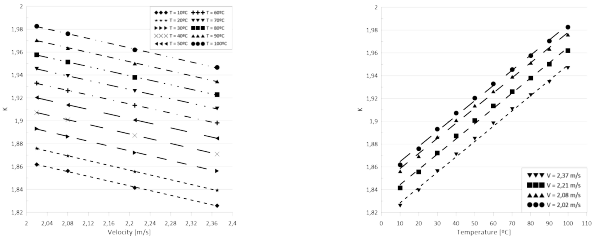

(a) K vs V. (b) K vs T.

Figure 7: Values of K for geometry A and their dependence on temperature and velocity.

Figure 7(a) presents the relation of K with the inlet velocity to all inlet temperatures. The values vary linearly with little error and show a similar tendency to previous works [6, 2]. The variation of K with the inlet temperature, shown in Figure 7(b), is also nearly linear for the four inlet velocities. It also shows a bigger influence of temperature in the values of K since there is a slightly higher slope in this graph. However, an increase in the local pressure loss coefficient for higher temperatures causes a decay in the energetic efficiency of the exhaust. The losses in energy to the colder walls (8(a)) also help to explain this tendency of K with temperature. Comparing to Figure 8(b), where is shown the velocity field for the same study, it is observed that in the recirculation zones, where the value for heat transfer coefficient peaks, the temperatures reach lower values easily. For the remaining zones, the temperature only decreases in a more significant way near the boundary layer zones, with the flow in the center of the channel barely varying.

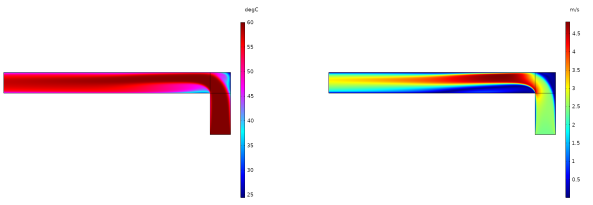

(a) Temperature results (b) Velocity results

Figure 8: Results of the simulation on geometry A for V_{max} and inlet temperature of 60°C.

For the studies for particle deposition, since particles can collide in different zones of the channel, it

was decided to name the different walls for a better interpretation of the problem (Figure 9).

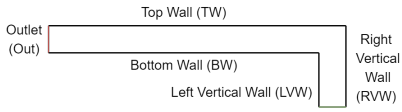

Figure 9: Wall nomenclature used in geometry A for the particle tracing study analysis.

Table 1: Deposition percentages for each diameter in geometry A with V_{max} and T = 20°C.

D_p	TW	Out	TCR	LVW	RVW
10	0	99.88	0.12	0	0
15	0	98.88	1.12	0	0
20	39.65	49	11.35	0	0
25	90.58	9.23	0.19	0	0
50	99.73	0	0	0	0.27
100	100	0	0	0	0

Firstly, the influence of the particle diameters is going to be seen. Table 1 presents the results of the particle tracing simulations for all diameters at maximum velocity, V = 2.37 m/s, and ambient temperature, T = 20°C. The results have equal tendencies to those obtained by Monteiro [2]: smaller particles are directly almost entirely to the outlet, which represents the filter in this work. This was expected because due to their very small mass, they also have a small Stokes number, following the streamlines of the flow and decreasing the chance of colliding with a wall or heading towards a recirculation zone. Bigger particles, with more mass and a bigger Stokes number, are more affected by their inertia and deviate from their original streamline easily. Hence, particles with a larger diameter get stuck in the wall closer to the entry zone. Notice that the filters in the real exhaust begin still in a zone represented in this study by the top wall, 27.5 mm away from the right vertical wall. This means that the further to the left the particle deposition is, the more particles the exhaust is able to capture efficiently. Particles with an intermediate size have a particularity: since the Stokes number is not as small, they deviate to some extent from the streamlines, which means that there is also a possibility to enter the top corner recirculation zone, being higher for bigger particles. However, once there, particles with more mass (higher Stokes number) have higher possibilities to leave the recirculation bubble. In this balance, turns out to be the particles with $D_p = 20$ μm the most likely to stay inside the bubble, with the particles of diameter $D_p = 50$ μm having a small possibility to end up in the right vertical wall while moving out of the recirculation zone.

The influence of inlet temperature and velocity is also analysed. With the studies for temperatures of 40°C and 60°C, one conclusion taken immediately is that the particle diameter has a much more significant dominance to define the deposition position of the particle itself. Nevertheless, the flow temperature still has some impact on the deposition places for the particles, specially for those with a diameter between 15 and 25 μm. Those particles tend slightly more towards the outlet and less towards the top wall as the temperature increases (coherent with Stokes number). A less dense flow (higher temperatures) also means it is easier for the particles to escape the recirculation zones. The results show a tendency by decreasing velocity similar to the one when the inlet temperature was increased to 60°C: much less significant comparing to the particle diameter and a tendency for more particles in the outlet and less in the top wall for the intermediate diameters. With a smaller flow velocity the particles in TCR also decreases, almost to none.

3.2. Geometric Alternatives

Two new geometries, B and C, were created. The idea for both of them was to reduce the recirculation zones and with it, the energy losses of the flow. This was made in different ways: in geometry B the approach was made by reducing the angle in the interior corner of the channel while in geometry C that corner was cut and divided in two smaller consecutive ones, while trying to eliminate the top corner recirculation zone. Figure 10 shows it was successful, and also a similar behaviour to geometry A for the temperature fields.

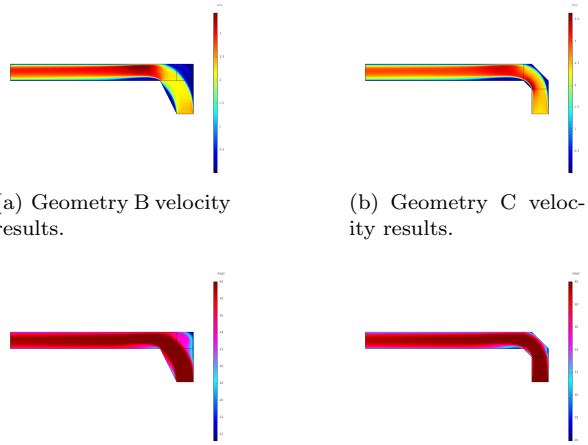

(a) Geometry B velocity results.

(b) Geometry C velocity results.

(c) Geometry B temperature results.

(d) Geometry C temperature results.

Figure 10: Flow velocities and temperatures for geometries B, C for the case of V_{max} and T = 40°C.

However, Geometry B shows a top corner recirculation area even bigger than in geometry A. This was expected, since the wall slope to the left allows

the flow to progress earlier to the exit zone, cornering with a less aggressive pressure gradient and leaving a bigger recirculation zone in the area to the right. However, the tendencies for temperature and velocity are still the same found in geometry A. Also visible in Figure 10 is the bottom recirculation bubble for each geometry. Their area is clearly inferior to the one in geometry A, as it was expected, with the tendency for the bottom recirculation length to peak at a certain Reynolds number still occurring (2800 to 2900 for geometry B, over 3350 for geometry C). The bottom recirculation length is slightly lower for geometry B. However, that geometry has a smaller bottom recirculation height (1.93 mm in geometry C against 2.17 mm in geometry B, for ambient temperature and maximum velocity). The tendencies for that value also remain the same from geometry A: a minimal drop with a decrease in velocity, with that peak height happening in the same section of the respective geometry, no matter the velocity.

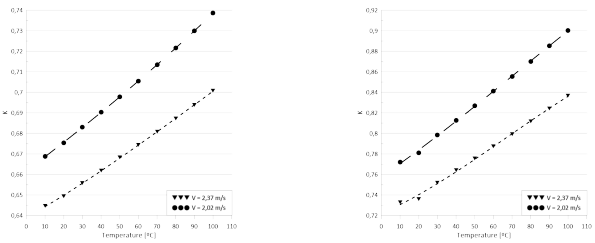

(a) Geometry B. (b) Geometry C.

Figure 11: Values of K for geometries B and C and their dependence on temperature and velocity.

The results for the local pressure loss coefficient K in both geometries are presented in Figure 11. The main conclusion to extract is that with the area reduction in the bottom recirculation zone, the new geometries successfully reduce the value of K. For an inlet temperature of T = 40°C at V_{max}, K decreases from 1.87 (geometry A) to 0.662 in geometry B and 0.690 in geometry C. Both cases still maintain the same linear tendencies with velocity and temperature shown in geometry A. The most efficient case is geometry B since the top corner recirculation zone does not absorb a lot of energy from the flow.

Being geometry B the most efficient of the two tested cases, it was chosen to be improved further. This was done by increasing the slope of the left entry wall, creating geometries B15, B20 and B30. Since the top corner recirculation zone seems not to absorb much energy from the flow, it is not going to be analysed. However, it is worth noticing that the tendencies were maintained. In these cases, only geometry B15 has a bottom recirculation zone, with a linear tendency across the inlet temperature variation. Its size is quite small comparing to previous geometries, with a length of 7.83 mm and maximum height of 0.37 mm for the case of maximum velocity and temperature of T = 20°C. For geometries B20 and B30, the bottom recirculation zone does not exist, replaced by another left to the entry. The only noticeable difference between both geometries is a bigger recirculation zone near the left entry wall for geometry B30, although it only increases by filling an area non-existent in geometry B20, with remaining flow path being nearly the same since the flow starts to behave similarly to a flow in a pipe with the same diameter of the exit zone even before entering that zone. That also happens in geometry B20, hence the disappearance of this recirculation bubble.

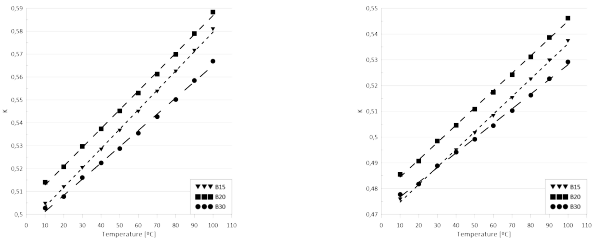

(a) K for V_{min}. (b) K for V_{max}.

Figure 12: Values of K for geometries B15, B20 and B30 and the dependence with temperature.

However, that flow behaviour on geometry B20 does not come across as desired in terms of values for K. With no recirculation zone in both geometries B20 and B30, the main difference in terms of losses occurs due to the extra 10 mm where the flow is in contact with the walls in the exit zone, meaning that geometry B30 has the upper hand in terms of K. Since the recirculation zone in geometry B15 is quite small, it does not take much energy from the flow. So, the values for K are also better in this case than for geometry B20. However, geometry B30 is still the best case overall, as it can be seen in Figure 12, although every case improves on geometry B due to the reduction or elimination of the bottom recirculation zone.

The new real cases for the exhaust geometry are now presented. Geometry D was still studied but some simulation cases were not converging since the short outlet was preventing the flow to reach a fully developed condition. Thus, only the results for geometry E will be presented. Comparing the top corner recirculation zone, it can be seen that the values for the wall lengths are slightly smaller than in geometry A. By removing the bottom wall of geometry A, it also allowed the bottom recirculation height to be smaller, comparing only in the 10 mm height of geometry A's exit zone: from 4.53 mm in geometry A to 4.25 mm in geometry E, for the same case (maximum inlet velocity and inlet tem-

perature of T = 20°C). This allows for the flow to pass through the bottleneck with less resistance and, possibly, less energy losses. It also explains the smaller area in the top corner recirculation zone. However, the removal of the bottom wall and attachment of a new area beneath it increases a lot the area of the bottom recirculation zone compared to geometry A, with the length going from 49.86 to 138.29 mm. This is visible in Figure 13.

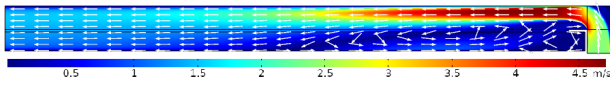

Figure 13: Flow velocities in geometry E for a case with V_{max} and T = 40°C.

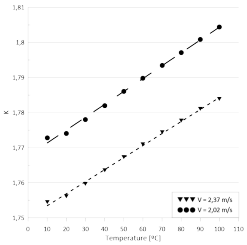

Figure 14: Values of K for geometry E and the variation with temperature and velocity.

The values for the local pressure loss coefficient, presented in the graph from Figure 14, reflect the discussion about the recirculation zones. The balance between a bottleneck that allows fluid to pass by easily and a bigger bottom recirculation zone results in a K value near (within the numerical uncertainty) but below the one in geometry A: for an inlet temperature of 20°C and inlet velocity of V = 2.37 m/s, geometry E presents a K of 1.76 while geometry A has a value of 1.84. The tendencies verified are still the same, with the only difference being a slower evolution of K with the inlet temperature. This behaviour can be partially explained due to the big difference between the geometries in the exit zone and because, since geometry E has a bigger channel height and length, the ratio of channel area to heated surface will be much larger, diminishing the temperature effects in the flow. Studies were made for the optimized versions of geometry E: E10, E15, E20 and E30 but the results for K were off from expected and far from any credible values since the simulations did not converge. For this reason, the results for these geometries will not be presented in this work.

For the particle deposition in these geometries, the same nomenclature from before will be used. Both new geometries B and C have the intended effect on the particle deposition: less particles end up in the walls and more in the outlet, and therefore, in the exhaust filter. This can be noticed very clearly particularly for the particles with a diameter of 20 μm. Another noticeable trend is the increase of particles in the top corner recirculation zone for geometry B, due to the increase in area for this recirculation bubble. This causes geometry C to have a slightly bigger percentage of particles on the outlet for some cases, since that geometry eliminates the bubble manifested in geometry B, replaced by two small negligible ones. However, geometry C has a higher percentage of particles on the top wall, with the particles of geometry B being deposited more to the left, closer to the zone where the filter begins in the real exhaust. Geometries B and C also keep the same tendencies from the initial geometry. Taking all of the previous inputs into consideration, it is concluded that geometry B has a better performance not only on an energetic level but also in terms of grease filtering efficiency.

Table 2: Deposition percentages for geometries B15, B20 and B30 with V_{max} and T = 40°C.

D_p	TW	Out	TCR	LEW	RVW
Geometry B15					
10	0	99.38	0.62	0	0
15	0	97.69	2.31	0	0
20	0	91.65	8.35	0	0
25	10.11	71.85	18.04	0	0
50	98.46	1.54	0	0	0
100	100	0	0	0	0
Geometry B20					
10	0	99.88	0.12	0	0
15	0	98.23	1.77	0	0
20	0	91.15	8.85	0	0
25	2.92	78.19	18.89	0	0
50	99.81	0.19	0	0	0
100	100	0	0	0	0
Geometry B30					
10	0	99.88	0.12	0	0
15	0	98.08	1.92	0	0
20	0	91.04	8.96	0	0
25	5.77	74.73	19.5	0	0
50	98.88	1.12	0	0	0
100	99.96	0.04	0	0	0

In geometries B15, B20 and B30, by increasing the left entry wall angle, the amount of particles entering the recirculation zone suffered a small increment. The pressure gradient affecting the flow also ends up being slightly reduced. This results in more particles going to the outlet and less particles deposited in the top wall for all the three geometries compared to geometry B, with the cases for geometries B20 and B30 being quite similar. Again, all previous tendencies for the particle deposition with particle diameter, flow inlet velocity and temperature were maintained and coherent with the Stokes

number influence on the particle movement. Although geometry B20 might have a small advantage in terms of particle deposition, it is the worse of the three geometries for pressure losses. So, geometry B30 is, from all the geometries studied in this work, the best case obtained for the two-phase flow of the exhaust.

For geometry E, the flow changes compared to geometry A by reducing the mass flow passing closer to the top wall, thus reducing the amount of deposition in the top wall while more particles are directed to the outlet, as intended. Due to the flow expansion caused by the height growth in the exit zone of the geometry, a very small amount of lighter particles ended up in the bottom wall for the simulations of geometry E. This is less likely to happen in the real exhaust because further ahead in the channel, the flow can start to be affected by an upstream from the exhaust pipe. Table 3 shows more in detail the numbers for the several particle deposition locations in geometry A and E, with all tendencies for property influence in particle movement and Stokes number still kept the same in this case.

Table 3: Deposition percentages for geometries A and E with V_{max} and T = 40°C.

D_p	TW	Out	TCR	LVW	RVW	BW
Geometry A						
10	0	99.84	0.12	0.04	0	0
15	0	99.15	0.85	0	0	0
20	32.65	62.08	5.27	0	0	0
25	78.31	14.69	7	0	0	0
50	99.73	0.12	0	0	0.15	0
100	100	0	0	0	0	0
Geometry E						
10	0	99.38	0.54	0	0	0.08
15	0	98.65	1.35	0	0	0
20	20.08	71.92	8	0	0	0
25	71.35	27.81	0.84	0	0	0
50	99.88	0.12	0	0	0	0
100	100	0	0	0	0	0

From this study, together with the small improvement in the values of K, it shows that the new geometry already implemented in the real exhaust might benefit the system. Although it does not perform better than the previous changes from this work, it shows that there exists potential to out-perform them by applying similar improvements.

3.3. Experimental Tests

To evaluate the numerical results from the studies performed in this work, it was carried out an experimental study as well. This was made in the acrylic prototype describe in Chapter 2.2, simulating the case of geometry B. Since only the minimum and maximum velocities were studied in the numerical part of this geometry, these were also the only cases tested experimentally. The tests were also performed at an ambient temperature around 25°C, being comparable to the inlet temperature of 20°C studied numerically.

The tests were performed in two different ways: the *single tube* method, where the data is retrieved by only one pitot tube in the outlet zone (similar to the tests conducted by Ferro [6]), and the *double tube* method, were pressure is measured both at the inlet and in the fully developed section. The graph below (Figure 15) displays the results for the local pressure loss coefficient K dependence on velocity on both cases and the numerical case as well.

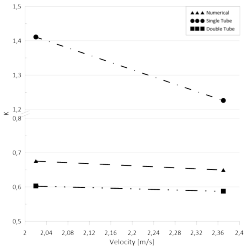

Figure 15: Values of K for experimental tests and numerical solution of geometry B at T = 20°C.

The results show the double tube method much closer to the numerical results than the single tube method, both for the dependence of K with velocity (with a much similar slope) and in terms of values, since the single tube method takes into account the dynamic pressure by considering atmospheric pressure at the inlet. This shows that assuming that the entry pressure is near the atmospheric pressure is an incorrect premise, leading to unexpectedly large values of K. The single tube method results are, however, coherent with the tests executed by Ferro since the values obtained numerically are around twice as high for geometry B but also for geometry A, the case tested in that said work. Comparing the results for the double tube method with the numerical, it looks that the simulations have similar results, keeping the tendency of a decreasing K value with the increase of the inlet velocity. Nonetheless, the numerical solution is overestimating the results of the experimental tests by around 10%. However, that is within the expected error range of the sensor for pressure values of this order. It should also be taken into account that, since the VARIAC works with an analog interface scale, the precision of the power used to control the flow velocity was far from ideal. The placing of the pitot tube at the inlet was also under optimized.

Nevertheless, the results being quite similar from the experimental to the numerical part of the work represents an improvement on previous works and the confirmation that the solutions can be correlated from numerical testing to reality.

4. Conclusions

This work had as an objective to improve the performance of a perimetric exhaust both on its energetic performance as well as on the grease filtering efficiency. For that, numerical studies were performed to a variety of new geometries in order to improve the initial geometry, reducing the energy lost in the flow and directing the grease particles to the exhaust filters, while taking into account the effects of the inlet velocity and working temperature of the flow. An experimental study was also performed for one of the geometries so the quality of the numerical simulations could be assessed.

The temperature of the flow entering the exhaust does have an influence on its functioning. Higher working temperatures result on a poorer energetic performance but in an increase on the grease filtering efficiency. The decrease in the inlet velocity has the same effect on energetic and grease filtering as the temperature increase, which is consistent with results from previous studies.

In the particle tracing studies, it was concluded that the property with more influence on the particle movement was the particle diameter. An increase on the particle size would cause it not to follow the flow streamlines as easily, with almost all heavier particles ending up on the top wall of the exhaust. On the other hand, a lighter particle follows perfectly the streamline, going to the filter. For the particles with intermediate sizes, working temperature and inlet velocity were decisive, with a temperature increase and velocity decrease favouring the particle movement towards the exhaust filter, represented in this study by the outlet.

Both geometry B and C, the first pair of geometries studied, have a considerably better performance than the initial geometry: the local pressure loss coefficient K values went down as much as three times for some of the studied cases and the number of particles in the outlet zone increase considerably for some particle diameters. However, it was geometry B that had the upper hand of the two. In order to improve geometry B, three modified versions were created from that foundation: geometries B15, B20 and B30. Although their evolution in performance wasn't linear with the increase in the slope of the wall throughout the versions, all of them were an improvement from the original geometry B. Geometries B20 and B30 were quite similar in terms of grease filtering efficiency due to the disappearance of the bottom recirculation zone present in every other geometry iteration but a lower energetic efficiency caused geometry B20 to be the worst of these final three geometry variations, with geometry B30 being the best performer energetically and, therefore, the overall best geometry in this work.

A new real case geometry was also studied in geometry E. Compared to the initial geometry A, a small improvement was found for the values of K, within the margin of numerical uncertainties, but with less dependence on the working temperature of the flow. It also improved slightly the grease filter efficiency, with a higher percentage of particles moving to the outlet due to a less narrow useful area for the flow to pass after the corner.

Finally, an experimental test was performed to a flow passing through an acrylic prototype channel with a corner based on geometry B. It was settled that the inlet pressure should also be measured instead of assuming atmospheric pressure at the entry, not taking into account the dynamic pressure at the entry. This test also confirmed the reliability of the numerical results, since the solutions obtained for both cases were similar.

Ending, it can be affirmed that the exhaust geometry improvement was accomplished, with the results suggesting that it is possible to obtain a significant improvement to the performance of the perimetric exhaust.

Acknowledgements

The author would like to thank Professors Edgar Caetano Fernandes and Luís Rego da Cunha de Eça, for all the guidance along this work.

References

[1] Teka DPE 90 Model. Image perimetric exhaust. Online; accessed 20-October-2019.

[2] Ivo Monteiro. Kitchen Exhauster channel numerical study and optimisation. Master's thesis, 2019.

[3] Frank M. White. *Fluid Mechanics*. McGraw-Hill, 7th edition, 2011.

[4] Thomas H Kuehn, Bernard a Olson, James W Ramsey, Joshua M Rocklage, and Deborah Gross. Characterization of effluents from additional cooking appliances. Technical report, 2007.

[5] A. Vié, H Pouransari, R Zamansky, and A. Mani. Comparison between Lagrangian and Eulerian methods for the simulation of particle-laden flows subject to radiative heating. *Center for Turbulence Researh, Annual Research Brief*, (i):15–25, 2014.

[6] Alexandre Ferro. Flows in suction channels of air exhausts. Master's thesis, 2018.